Frédéric Waldmann, Christof Baeriswyl, Raphael Andonie, and Reto A. Wildhaber*

Onset Detection of Pulse-Shaped Bioelectrical Signals Using Linear State Space Models

https://doi.org/10.1515/cdbme-2022-1027

Abstract: Bioelectrical signals are often pulse-shaped with superimposed interference signals. In this context, accurate identification of features such as pulse onsets, peaks, amplitudes, and duration is a frequent problem. In this paper, we present a versatile method of rather low computational complexity to robustly identify such features in real-world signals. For that, we take use of two straight-line models fit to the observations by minimizing a quadratic cost term, and then identify desired features by tweaked likelihood measures. To demonstrate the idea and facilitate access to the method, we provide examples from the field of cardiology.

Keywords: linear state space models, recursive least squares, likelihood, feature extraction, onset detection, ecg waves

1 Introduction

Robust detection of features such as onsets, peaks, or duration of pulses in noisy bioelectrical signals are essential tasks that have not yet definitely been solved. Well-known examples for these kind of problems are the identification of electrocardiography (ECG) wave characteristics such as QRS, P, and T waves [1–4].

In this paper, we propose a different approach based on squared error optimization and recursively computed signal models: we use two straight-line models, which are fit to the observations in a recursive least squares manner using autonomous linear state space models [5].

Frédéric Waldmann, Institute for Medical Engineering and Medical Informatics, University of Applied Sciences and Arts Northwestern Switzerland, Muttenz, Switzerland
Christof Baeriswyl, STADIUS Center for Dynamical Systems, Signal Processing and Data Analytics, KU Leuven, Leuven, Belgium, and Bern University of Applied Sciences, Biel, Switzerland
Raphael Andonie, Hearing Research Laboratory, ARTORG Center for Biomedical Engineering Research, University of Bern, Bern, Switzerland.
***Corresponding author: Reto A. Wildhaber,** Institute for Medical Engineering and Medical Informatics, University of Applied Sciences and Arts Northwestern Switzerland, Hofackerstrasse 30, Muttenz, Switzerland, and ETH Zurich, Sternwartstrasse 7, Zurich, Switzerland, reto.wildhaber@fhnw.ch

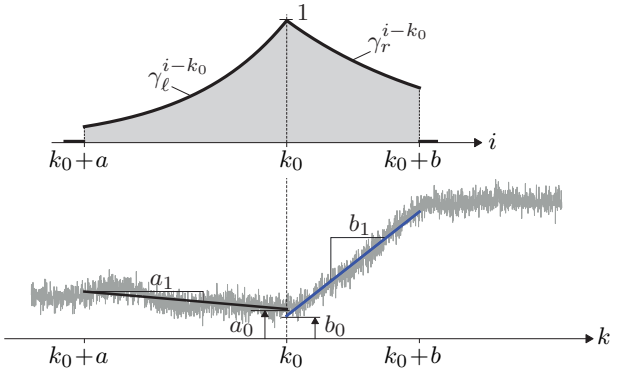

Fig. 1: Illustration of a Two-Sided Line Model (TSLM), as in (19), fit to noisy observations around time index k_0. The two-sided exponentially decaying window (upper plot) localizes the fit to the range k_0+a to k_0+b. The left line segment of the TSLM (black line, lower plot) approximates the observations from k_0+a to k_0-1, with line offset a_0 and slope a_1; the right line segment of the TSLM (blue line) fits from k_0 to k_0+b, with b_0 and b_1 accordingly.

2 ALSSMs as Signal Models

We use discrete-time Autonomous Linear State Space Models (ALSSMs) to generate generic straight line models. ALSSMs are defined recursively as

$$x_{j+1} = Ax_j \tag{1}$$

$$s_j = cx_j \tag{2}$$

with transition matrix $A \in \mathbb{R}^{N\times N}$, output vector $c \in \mathbb{R}^{1\times N}$, output $s_j \in \mathbb{R}$, state vector $x_j \in \mathbb{R}^N$, and initialized at index $j = 0$ by initial state x_0, subsequently simply denoted as x. This often leads to efficiently computable quadratic cost terms.

Such ALSSMs can generate a wide field of signal shapes [5]. However, here we use solely straight lines. To generate a line of offset a_0 and slope a_1, we introduce the ALSSM of order $N = 2$ of configuration

$$A = \begin{bmatrix} 1 & 1 \\ 0 & 1 \end{bmatrix}, \quad c = \begin{bmatrix} 1 & 0 \end{bmatrix}, \tag{3}$$

with initial state

$$x = \begin{bmatrix} a_0 & a_1 \end{bmatrix}^\mathsf{T} \in \mathbb{R}^2 . \tag{4}$$

Substituting (1) in (2) and using the ALSSM as in (3) leads to the closed form of the straight-line model, with x as in (4),

$$s_j(x) = cA^j x = a_0 + a_1 j \quad \in \mathbb{R} . \tag{5}$$

To now locally fit such a line model to an observed signal vector $y \in \mathbb{R}^K$, $K \in \mathbb{N}$, over the interval $\{k+a, \ldots, k+b\}$, $a, b \in \mathbb{Z}$, $a < b$, we need to minimize the quadratic cost

$$J_a^b(x, \gamma, k) \triangleq \sum_{i=k+a}^{k+b} \gamma^{i-k} \big[y_i - s_{i-k}(x)\big]^2 \quad \in \mathbb{R}_+ \,. \quad (6)$$

Parameter $\gamma \in \mathbb{R}$ introduces an exponential decay to the applied window located around k. This is an additional design parameter, summarized in Tab. 1, which is essential for numerical stability in recursive computations such as we introduce later. The optimal state $\hat{x}_k$ (holding a_0 and a_1) minimizing the quadratic cost (6) is, in accordance to [5],

$$\hat{x}_k = \underset{x}{\operatorname{argmin}} \sum_{i=k+a}^{k+b} \gamma^{i-k} \big[y_i - s_{i-k}(x)\big]^2 \quad (7)$$

$$= \underset{x}{\operatorname{argmin}} \big[x^\mathsf{T} W_k x - 2x^\mathsf{T} \xi_k + \kappa_k\big] \quad (8)$$

$$= W_k^{-1} \xi_k \quad (9)$$

with the substitutes

$$\kappa_k = \textstyle\sum_{i=k+a}^{k+b} \gamma^{i-k} y_i^2 \;\in \mathbb{R} \quad (10)$$

$$\xi_k = \textstyle\sum_{i=k+a}^{k+b} \gamma^{i-k} \big(A^\mathsf{T}\big)^{i-k} c^\mathsf{T} y_i \;\in \mathbb{R}^N \quad (11)$$

$$W_k = \textstyle\sum_{i=k+a}^{k+b} \gamma^{i-k} \big(A^\mathsf{T}\big)^{i-k} c^\mathsf{T} c A^{i-k} \;\in \mathbb{R}^{N\times N} \,. \quad (12)$$

From [5], we know that recursive computation rules exist for (10) to (12): The forward recursion $k \to k+1$ is

$$\kappa_{k+1} = \gamma^{-1}\kappa_k - \gamma^{a-1} y_{k+a}^2 + \gamma^b y_{k+b+1}^2 \quad (13)$$

$$\xi_{k+1} = \gamma^{-1} A^{-\mathsf{T}} \xi_k - \gamma^{a-1} \big(A^{a-1}\big)^\mathsf{T} c^\mathsf{T} y_{k+a} + \gamma^b \big(A^b\big)^\mathsf{T} c^\mathsf{T} y_{k+b+1} \quad (14)$$

$$W_{k+1} = \gamma^{-1} A^{-\mathsf{T}} W_k A^{-1} - \gamma^{a-1} \big(A^{a-1}\big)^\mathsf{T} c^\mathsf{T} c A^{a-1} + \gamma^b \big(A^b\big)^\mathsf{T} c^\mathsf{T} c A^b \,, \quad (15)$$

or alternatively, the backward recursions $k \to k-1$ is

$$\kappa_{k-1} = \gamma\kappa_k + \gamma^a y_{k+a-1}^2 - \gamma^{b+1} y_{k+b}^2 \quad (16)$$

$$\xi_{k-1} = \gamma A^\mathsf{T} \xi_k + \gamma^a \big(A^a\big)^\mathsf{T} c^\mathsf{T} y_{k+a-1} - \gamma^{b+1} \big(A^{b+1}\big)^\mathsf{T} c^\mathsf{T} y_{k+b} \quad (17)$$

$$W_{k-1} = \gamma A^\mathsf{T} W_k A + \gamma^a \big(A^a\big)^\mathsf{T} c^\mathsf{T} c A^a - \gamma^{b+1} \big(A^{b+1}\big)^\mathsf{T} c^\mathsf{T} c A^{b+1} \,. \quad (18)$$

3 Two-Sided Straight Line Model

Over the years of working with bioelectrical signals, it has become evident that a Two-Sided Line Model (TSLM) in a squared error framework is a versatile tool for detecting various types of change points in observed signals. Such change points include: changes in signal slopes, jumps, pulse onsets, pulse endings. Our TSLMs are composed of two lines, both as introduced in (5). The left line segment points from a reference index k to the left, i.e., from $k+a$ to $k-1$ (with $a \le -1$), and the right line points from the same index k to the right, i.e., from k to $k+b$ (with $b \ge 0$). Figure 1 illustrates this arrangement. So, the cost term to fit a TSLM to an observed signal y at reference index k is

$$\widetilde{J}\Big(\Big[\tfrac{x_\ell}{x_r}\Big], k\Big) \triangleq J_a^{-1}(x_\ell, \gamma_\ell, k) + J_0^b(x_r, \gamma_r, k) \quad (19)$$

with the independent states for the left- and right-sided model

$$x_\ell = \begin{bmatrix} a_0 \\ a_1 \end{bmatrix} \in \mathbb{R}^2 \quad , \quad x_r = \begin{bmatrix} b_0 \\ b_1 \end{bmatrix} \in \mathbb{R}^2 \quad (20)$$

where a_0 and a_1 are offset and slope of the left-sided line segment, and b_0 and b_1 offset and slope of the right-sided line segment, respectively, see Fig. 1.

The estimates of the four independent states then are

$$\hat{x}_\ell = \underset{x_\ell}{\operatorname{argmin}}\, J_a^{-1}(x_\ell, \gamma_\ell, k) \quad (21)$$

$$\hat{x}_r = \underset{x_r}{\operatorname{argmin}}\, J_0^b(x_r, \gamma_r, k) \,, \quad (22)$$

with closed form solution (9). An example fit is also illustrated in Fig. 1.

We note that the two line segments are not necessarily continuous, since $\hat{x}_\ell$ and $\hat{x}_r$ are estimated independently. However, to force continuity of the two line segments, we introduce a linear constraint of the general form

$$\Big[\tfrac{x_\ell}{x_r}\Big] = Hv \quad \in \mathbb{R}^4 \quad (23)$$

to the states with constraint matrix $H \in \mathbb{R}^{4\times M}$ and independent states $v \in \mathbb{R}^M$, $M \le 4$. (M here denotes the number of remaining independent states to be estimated.)

For example, to force continuity in the two lines, i.e., $a_0 = b_0$, we introduce a linear constraint (23),

$$\Big[\tfrac{x_\ell}{x_r}\Big] = Hv = \underbrace{\begin{bmatrix} 1 & 0 & 0 \\ 0 & 1 & 0 \\ 1 & 0 & 0 \\ 0 & 0 & 1 \end{bmatrix}}_{H} \underbrace{\begin{bmatrix} a_0 \\ a_1 \\ \hline b_1 \end{bmatrix}}_{v} \,. \quad (24)$$

Tab. 1: Infinite and finite windows with exponential decay.

$\gamma_\ell, \gamma_r \in \mathbb{R}; a, b \in \mathbb{Z}$	**Left Segment**	**Right Segment**
Infinite Support Window $a \to -\infty, \gamma_\ell > 1.0$ $b \to +\infty, \gamma_r < 1.0$	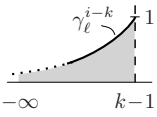	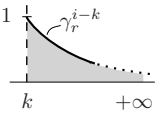
Finite Support Window $a \le -1, \gamma_\ell > 1.0$ $b \ge 0, \gamma_r < 1.0$	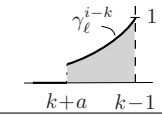	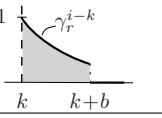
Rectangular Window[1] $a \le -1, \gamma_\ell = 1.0 + \epsilon$ $b \ge 0, \gamma_r = 1.0 - \epsilon$ ($\epsilon \approx 0.00001 \ldots 0.01$)	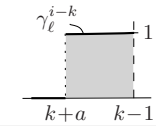	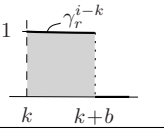

[1] Rectangular windows are an important special case of Finite Support Windows. Note that ϵ is essential for numerical stability.

Tab. 2: Useful linear constraints for TSLMs.

$a_0, a_1, b_0, b_1 \in \mathbb{R}$	$H \in \mathbb{R}^{N\times M}$	**Example**
"Free" (Unconstrained)	$\left[\begin{array}{cc\|cc} 1&0&0&0\\ 0&1&0&0\\ \hline 0&0&1&0\\ 0&0&0&1 \end{array}\right]$	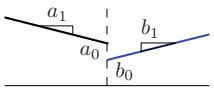
"Continuous" $a_0 = b_0$	$\left[\begin{array}{ccc} 1&0&0\\ 0&1&0\\ \hline 1&0&0\\ 0&0&1 \end{array}\right]$	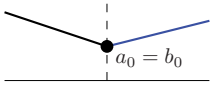
"Straight" $a_0 = b_0$ $a_1 = b_1$	$\left[\begin{array}{cc} 1&0\\ 0&1\\ \hline 1&0\\ 0&1 \end{array}\right]$	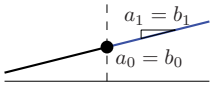
"Horizontal" $a_0 = b_0$ $a_1 = b_1 = 0$	$\left[\begin{array}{c} 1\\ 0\\ \hline 1\\ 0 \end{array}\right]$	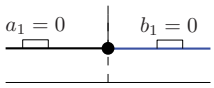
"Left Horizontal" $a_0 = b_0$ $a_1 = 0$	$\left[\begin{array}{cc} 1&0\\ 0&0\\ \hline 1&0\\ 0&1 \end{array}\right]$	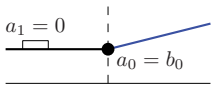
"Right Horizontal" $a_0 = b_0$ $a_1 = 0$	$\left[\begin{array}{cc} 1&0\\ 0&1\\ \hline 1&0\\ 0&0 \end{array}\right]$	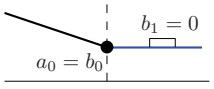
"Peak" $a_0 = b_0$ $a_1 = -b_1$	$\left[\begin{array}{cc} 1&0\\ 0&1\\ \hline 1&0\\ 0&-1 \end{array}\right]$	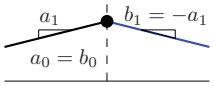
"Step" $a_1 = b_1 = 0$ $(\Delta = b_0 - a_0)$	$\left[\begin{array}{cc} 1&0\\ 0&0\\ \hline 0&1\\ 0&0 \end{array}\right]$	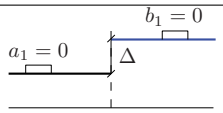

Vector $v \in \mathbb{R}^3$ holds the M remaining independent variables a_0, a_1, and b_1, while b_0 is bound to a_0. This and further examples of common linear constraints are summarized in Tab. 2.

To minimize the cost (19) with respect to such constraints, we first reparametrize (19), in analogy to (8), as

$$\begin{aligned}\widetilde{J}\left(\begin{bmatrix}x_\ell\\ x_r\end{bmatrix}, k\right) &= \left(x_\ell^\mathsf{T}\overrightarrow{W}_k x_\ell - 2x_\ell^\mathsf{T}\overrightarrow{\xi}_k + \overrightarrow{\kappa}_k\right) + \left(x_r^\mathsf{T}\overleftarrow{W}_k x_r - 2x_r^\mathsf{T}\overleftarrow{\xi}_k + \overleftarrow{\kappa}_k\right)\\ &= \left(\begin{bmatrix}x_\ell\\ x_r\end{bmatrix}^\mathsf{T}\widetilde{W}_k\begin{bmatrix}x_\ell\\ x_r\end{bmatrix}\right) - 2\begin{bmatrix}x_\ell\\ x_r\end{bmatrix}^\mathsf{T}\widetilde{\xi}_k + (\overrightarrow{\kappa} + \overleftarrow{\kappa}) \qquad (25)\end{aligned}$$

with

$$\widetilde{\xi}_k = \begin{bmatrix}\overrightarrow{\xi}_k\\ \overleftarrow{\xi}_k\end{bmatrix} \in \mathbb{R}^{4\times 1}, \quad \widetilde{W}_k = \left[\begin{array}{c|c} \overrightarrow{W}_k & 0\\ \hline 0 & \overleftarrow{W}_k\end{array}\right] \in \mathbb{R}^{4\times 4}, \quad (26)$$

and with $\overrightarrow{\xi}_k$ and $\overrightarrow{W}_k$ corresponding to (14) and (15) from the left side segment, and $\overleftarrow{\xi}_k$ and $\overleftarrow{W}_k$ (17) and (18) from the right side segment, accordingly. To minimize (25) with respect to the constraint (23), we first substitute (23) in (25), leading to the optimum solution

$$\hat{v}_k = (H^\mathsf{T}\widetilde{W}_k H)^{-1} H^\mathsf{T}\widetilde{\xi}_k \quad \in \mathbb{R}^M, \qquad (27)$$

and finally again to the full state vectors

$$\begin{bmatrix}\hat{x}_\ell\\ \hat{x}_r\end{bmatrix}_k = H\hat{v}_k \quad \in \mathbb{R}^4. \qquad (28)$$

The full derivation of (27) is given in [5].

4 Log-Cost Ratio (LCR)

We use log-cost ratios (LCRs) to robustly detect events. A cost ratio is the counterpart to a likelihood measure in statistics, which measures the likelihood of two alternative hypotheses [6]. Therefore, we compare two alternative costs (25) with distinct constraints: a desired hypothesis $\widetilde{J}(H_1 v, k)$ versus an alternative or null hypothesis $\widetilde{J}(H_0 v, k)$. We consider the ratio

$$\mathrm{LCR}_k = -\frac{1}{2}\log\frac{\min\limits_v \widetilde{J}(H_1 v, k)}{\min\limits_v \widetilde{J}(H_0 v, k)} \quad \in \mathbb{R}. \qquad (29)$$

The log-scale in (29) is also borrowed from statistics and leads to a better readability when displayed graphically, while preserving minima and maxima values. Finally, LCR_k peaks whenever the desired hypothesis and its associated event have maximum local likelihood. Figure 2 shows an example of a likelihood measure detecting edges in a signal.

5 Examples

5.1 Basic Detection Example

A trivial first example illustrates the detection of edges using a TSLM, weighting the two options of a "Continuous" versus a "Straight" line (cf. Tab. 2) in a LCR term, see Fig. 2. For this example, the following TSLM parameters apply:

Task	Left Segment	Right Segment	Log-Cost Ratio
Edge	$\gamma_\ell = 1.01$ $a = -200$	$\gamma_r = 1/\gamma_\ell = 0.99$ $b = -a - 1 = 199$	H_1 : "Continuous" H_0 : "Straight"

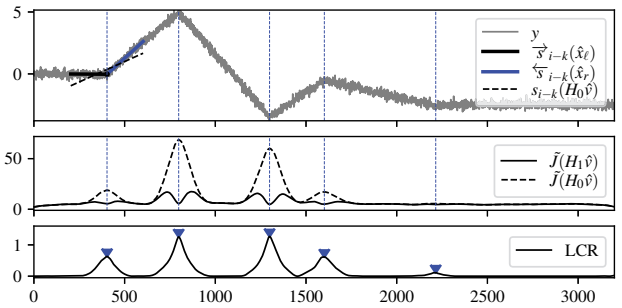

Fig. 2: Upper plot: TSLM (black/blue) and synthetic noisy signal (gray line) with abrupt changes in slope. Center plot: squared error cost of the desired hypothesis "Continuous" TSLM (solid black) and alternative hypothesis "Straight" TSLM (dashed). Bottom plot: LCR weighting the two hypotheses against each other, cf. Ex. 5.1.

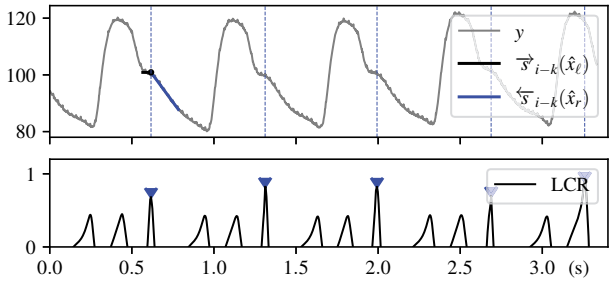

Fig. 3: Upper plot: arterial blood pressure signal recorded at $f_s = 600\,\mathrm{Hz}$. Lower plot: LCR value with marked peaks, indicating the detected dicrotic notches (blue triangles), cf. Ex. 5.2.

5.2 Dicrotic Notch Detection in ABP

Arterial blood pressure (ABP) signals usually show a dicrotic notch in the decreasing slope which are considered as the end of a systolic cycle, cf. Fig. 3. To detect these notches, we use a TSLM model with the following parameters (at $f_s = 600\,\mathrm{Hz}$):

Task	Left Segment	Right Segment	Log-Cost Ratio
Notch	$\gamma_\ell = 1.01$ $a = -30$	$\gamma_r = 1/\gamma_\ell = 0.99$ $b = 100$	H_1 : "Left Horizontal" H_0 : "Straight"

Figure 3 shows the resulting LCR with the detection result.

5.3 P and T Wave Detection in ECG

Another common task in cardiology is to accurately measure onsets and peaks of P and T waves in the electrocardiography (ECG) signals. To robustly extract these features, we parametrize our TSLMs as follows (at $f_s = 500\,\mathrm{Hz}$):

Task	Left Segment	Right Segment	Log-Cost Ratio
Onset	$\gamma_\ell = 1.01$ $a = -80$	$\gamma_r = 1/\gamma_\ell = 0.99$ $b = 40$	H_1 : "Left Horizontal" H_0 : "Horizontal"
Peak	$\gamma_\ell = 1.01$ $a = -45$	$\gamma_r = 1/\gamma_\ell = 0.99$ $b = -a - 1 = 44$	H_1 : "Peak" H_0 : "Horizontal"

Figure 4 illustrates the method applied on an ECG sequence.

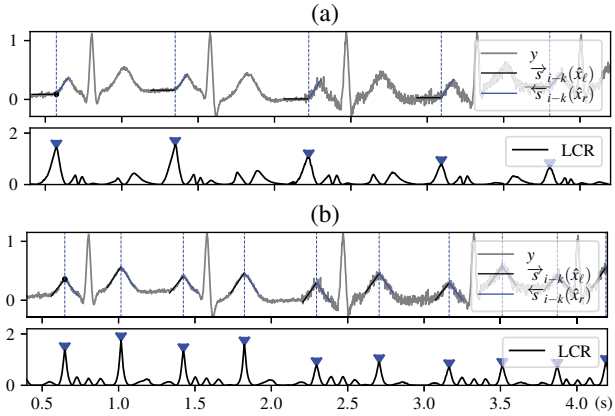

Fig. 4: The figure shows robust detection of (a) P wave onsets, and (b) P and T wave peaks, both in a noisy ECG signal recorded at sampling rate $f_s = 500\,\mathrm{Hz}$, cf. Ex. 5.3. To demonstrate the robustness of the method, artificial white Gaussian noise is added to the ECG after $t = 2.2\,\mathrm{s}$.

6 Conclusion & Final Remarks

We have presented a simple, yet powerful method for detecting features in pulse-shaped signals, such as bioelectrical recordings. The methods have proven to be useful and flexible in various clinical projects in recent years, especially in devices where extensive computing power is not available.

In the examples presented, the parameters of the TSLMs were intuitively selected. The features of interest were localized by identifying local maxima in the LCR (after specifying a minimum value and distance for valid LCR peaks to roughly filter out invalid detections). However, to avoid false detections and increase robustness of the algorithms, in practice it is advantageous use a smaller search window synchronized by an easily detectable feature (e.g., by systolic peaks or the QRS). For the sake of simplicity, we have avoided this enhancement in our presented examples.

The source code for all example is available online [7].

Author Statement

Research funding: R. A. Wildhaber receives financial support from Solothurner Spitäler, Switzerland. Conflict of interest: Authors state no conflict of interest. Ethical approval: The research related to human use complies with all the relevant national regulations, institutional policies and was performed in accordance with the tenets of the Helsinki Declaration, and has been approved by the authors' institutional review board or equivalent committee.

References

[1] B. U. Kohler, C. Hennig, and R. Orglmeister, "The principles of software QRS detection," *IEEE Engineering in Medicine and Biology Magazine*, vol. 21, no. 1, pp. 42–57, Jan. 2002.

[2] J. P. Martínez, R. Almeida, S. Olmos, A. P. Rocha, and P. Laguna, "A wavelet-based ecg delineator: evaluation on standard databases," *IEEE Transactions on biomedical engineering*, vol. 51, no. 4, pp. 570–581, 2004.

[3] J. Pan and W. J. Tompkins, "A real-time qrs detection algorithm," *IEEE transactions on biomedical engineering*, no. 3, pp. 230–236, 1985.

[4] C. Li, C. Zheng, and C. Tai, "Detection of ecg characteristic points using wavelet transforms," *IEEE Transactions on biomedical Engineering*, vol. 42, no. 1, pp. 21–28, 1995.

[5] R. A. Wildhaber, N. Zalmai, M. Jacomet, and H.-A. Loeliger, "Windowed state-space filters for signal detection and separation," *IEEE Transactions on Signal Processing*, vol. 66, no. 14, pp. 3768–3783, 2018.

[6] N. Zalmai, "A state space world for detecting and estimating events and learning sparse signal decompositions," Ph.D. dissertation, ETH Zurich, 2017.

[7] R. A. Wildhaber, F. Waldmann, and L. Fleischmann. (2022) lmlib - an open source model-based signal processing library. Website. [Online]. Available: http://lmlib.ch